

Precise Construction of Nitrogen-Enriched Porous Ionic Polymers as Highly Efficient Sulfur Dioxide Adsorbent

Sen Chen, Shicheng Huang, Zhenglu Yang, Xian Suo,* Huabin Xing, and Xili Cui*

Porous ionic polymers with unique features have exhibited high performance in various applications. However, the fabrication of functional porous ionic polymers with custom functionality and porosity for efficient removal of low-concentration SO₂ remains challenging. Herein, a novel nitrogen-enriched porous ionic polymer NH₂Py-PIP is prepared featuring high-content nitrogen sites (15.9 wt.%), adequate ionic sites (1.22 mmol g⁻¹), and a hierarchical porous structure. The proposed construction pathway relies on a tailored nitrogen-functionalized cross-linker NH₂Py, which effectively introduces abundant functional sites and improves the porosity of porous ionic polymers. NH₂Py-PIP with a well-engineered SO₂-affinity environment achieves excellent SO₂/CO₂ selectivity (1165) and high SO₂ adsorption capacity (1.13 mmol g⁻¹ at 0.002 bar), as well as enables highly efficient and reversible dynamic separation performance. Modeling studies further elucidate that the nitrogen sites and bromide anions collaboratively promote preferential adsorption of SO₂. The unique design in this work provides new insights into constructing functional porous ionic polymers for high-efficiency separations.

1. Introduction

Porous ionic polymers, as an intriguing class of porous materials, combine the merits of both ionic materials and porous polymers.^[1] These materials exhibit intrinsic properties including unique ionic environment, appealing structural diversity, tunable pore structure, and excellent physicochemical stability, marking them as promising candidates for a wide range of applications.^[2] In the rapidly evolving field of these materials, significant progress has been made in areas such as

separation, catalysis, and energy storage, covering applications like sulfur dioxide (SO₂) removal, carbon capture, and hydrocarbon separation.^[3] Functionalizing porous ionic polymers with specific targets offers abundant opportunities for high-performance applications. The functionalization strategies could be mainly classified into two categories. Direct synthesis derived from functional monomers represents a common approach for decorating pore walls. For example, porous poly(ionic liquid) is directly prepared via polymerization using ionic monomers with functionalized anions or cations, synthesis reaction, and pore formation concurrently occur by exploiting this route.^[4] However, strong electrostatic interactions between abundant ionic pairs in the polymer network with a soft nature would lead to densely packed ionic chains and an undeveloped porous structure. Another facile method is post-modification, such

as anion exchange and impregnation of functional compounds, which introduces tailored groups mostly via chemical reaction or physical loading.^[5] Limited by the network structure and steric hindrance obstacle of the porous precursors, the post-modification process cannot proceed completely, resulting in low-content targeted moieties, especially for multi-functionalization. In addition, the pore accessibility of as-formed polymer is inevitably decreased due to additional groups occupying the pore cavity. Therefore, there is a requirement to develop a new synthetic methodology for functional porous ionic polymers, to overcome the trade-off between functionality and porosity.

Target-motivated functionalization of porous ionic polymers enables the deployment of task-specific applications like important gas separation, for which specific sites help to achieve efficient removal of impurities and selective separation of structurally similar systems.^[6] Low-concentration SO₂ capture is a crucial process in flue gas desulfurization, the residual SO₂ could react with organo-amines during the CO₂-scrubbing process and poison the noble catalyst in important industrial processes. Traditional capture technology often results in low removal efficiency and environmental pollution.^[7] Considerable effort has been dedicated to constructing porous materials for promising SO₂ adsorptive capture.^[8] However, precise recognition of SO₂ in the presence of carbon dioxide (CO₂), which has a very similar structure and acidic properties, remains a significant challenge.^[9] Several reported ionic polymers have achieved

S. Chen, S. Huang, Z. Yang, X. Suo, H. Xing, X. Cui
Engineering Research Center of Functional Materials Intelligent
Manufacturing of Zhejiang Province
Department of Chemical and Biological Engineering
Zhejiang University
Hangzhou 310012, China
E-mail: xiansuo@zju.edu.cn; cuixl@zju.edu.cn

S. Chen, Z. Yang, X. Suo, H. Xing, X. Cui
ZJU-Hangzhou Global Scientific and Technological Innovation Center
Hangzhou 311215, China
X. Cui
Shanxi-Zheda Institute of Advanced Materials
Chemical Engineering
Hangzhou 310027, China

 The ORCID identification number(s) for the author(s) of this article can be found under <https://doi.org/10.1002/sml.202400746>

DOI: 10.1002/sml.202400746

selective SO₂ capture comparable to those of top-performing materials such as metal–organic frameworks (MOFs), and porous organic polymers (POPs).^[10] However, there are still a few ionic polymers affording high selectivity and capacity.^[11] For example, the ionic microgel P(D[VImC₆]Br),^[12] which was directly synthesized from ionic monomers, exhibited good SO₂/CO₂ uptake selectivity (614) but afforded negligible SO₂ uptake at low concentration (0.1 mmol g⁻¹ at 0.002 bar), arising from nonporous structure. Another example was the ionic porous organic framework Viologen-POF,^[13] in which high SO₂ capacity (1.45 mmol g⁻¹ at 0.002 bar) was achieved with moderate SO₂/CO₂ uptake selectivity (467) due to the lack of specific functionality. The introduction of SO₂-affinity sites, such as basic nitrogen sites, and carboxylic acid/carboxylate sites, can bestow porous ionic polymers with enhanced separation efficiency, and a well-defined porous structure can promote gas adsorption ability.^[15] Existing porous ionic polymers have been almost fabricated from common ionic units, which are seldom decorated with recognition groups. Moreover, combining ample functional sites and porosity is still challenging, limiting their applicability in highly efficient SO₂ removal.

Herein, we prepared a new kind of nitrogen-enriched porous ionic polymer, NH₂Py-PIP (NH₂Py denotes 3,5-divinylpyridin-2-amine, PIP denotes porous ionic polymer), via a facile functionalization methodology based on nitrogen-functionalized cross-linker NH₂Py for the first exploration. Unexpectedly, this material not only exhibits distinctive functional characteristics including high nitrogen content (15.9 wt.%) and abundant ionic sites (1.22 mmol g⁻¹) but also possesses well-developed hierarchical porosity. Benefiting from precise control of the pore chemistry and structure, NH₂Py-PIP realizes efficient SO₂ capture with high SO₂/CO₂ selectivity (1165) and satisfactory SO₂ adsorption capacity (1.13 mmol g⁻¹, 0.002 bar). This material presents outstanding dynamic separation performance with good recyclability during the removal of low-concentration SO₂, as demonstrated by breakthrough experiments. Molecular simulation results elucidate that the abundant nitrogen sites and bromide anions play vital roles in distinguishing SO₂ and CO₂, promoting high-performance SO₂ capture.

2. Results and Discussion

2.1. Preparation and Characterization

In this work, to fabricate a kind of porous ionic polymers for SO₂ removal, a nitrogen-functionalized cross-linker NH₂Py, which possesses SO₂-affinity sites on the amino and pyridine groups, was judiciously selected. The nitrogen-enriched ionic porous polymer NH₂Py-PIP was successfully constructed via copolymerization of NH₂Py and an ionic liquid (IL) monomer 1-vinyl-3-ethylimidazolium bromide ([EVIM][Br]) (Figure 1). The chemical structure of NH₂Py-PIP was confirmed by Fourier transform infrared (FTIR) spectroscopy, solid-state ¹³C nuclear magnetic resonance (NMR) spectroscopy, and X-ray photoelectron Spectroscopy (XPS) (Figure 1B; Figures S19 and S20, Supporting Information). In FTIR spectroscopy, the peaks at 3380 and 1568 cm⁻¹ belong to the N–H stretching vibrations of the amine group in the pyridine ring, and a peak corresponding to the stretching vibrations of the C=C bonds in the pyridine ring and imidazole ring appears at 1618 cm⁻¹, which proves the introduc-

tion of NH₂Py. The introduction of imidazolium-based cations is confirmed by the presence of a peak at 1154 cm⁻¹ representing the C–N characteristic peak in imidazole cations, and the peak observed at 1467 cm⁻¹ is ascribed to the stretching vibration of C=N in the pyridine ring and the stretching and bending vibrations of the methyl groups in ILs. An elemental analysis experiment of the ionic porous polymer was carried out to quantitatively evaluate the pore microenvironment feature. Excitingly, NH₂Py-PIP presents a high nitrogen content of up to 15.90 wt.% and an adequate IL content of 1.22 mmol g⁻¹ (Table S1, Supporting Information). NMR spectroscopy shows a distinct peak at 155 ppm is attributed to amino-substituted pyridine carbons, suggesting the incorporation of NH₂Py into the polymer skeleton (Figure S19, Supporting Information). The presence of the Br element in the XPS result further proves the introduction of [EVIM][Br], and the nitrogen content value (13.0 wt.%) was close to the elemental analysis results. For further analyzing the task-specific functionalization, we prepared the material DVB-PIP for comparison, which was obtained from the common cross-linker divinyl benzene (DVB) without functional sites. The as-synthesized DVB-PIP affords total nitrogen sites as low as 0.29 wt.% and very few ionic liquid sites (0.21 mmol g⁻¹). The obvious difference in functionality between NH₂Py-PIP and DVB-PIP is also displayed in the FTIR spectra (Figure 1B). These results demonstrate that exploitation of the cross-linker NH₂Py achieves the successful incorporation of ample nitrogen sites while promoting ionic moiety into the polymer network.

To sufficiently analyze the pore structure properties of these porous ionic polymers, argon (Ar) sorption isotherms were measured at 87 K (Figure 1C; Figure S1, Supporting Information). The Ar isotherm of NH₂Py-PIP exhibits apparent uptake at low relative pressure (P/P₀) below 0.01, indicative of a microporous structure, and the calculated microporous surface area is 200.1 m² g⁻¹ based on the t-plot method. Additionally, there is a remarkable increase at a high P/P₀ above 0.4, indicating the existence of a meso-macroporous structure. The Brunauer–Emmett–Teller (BET) surface area (S_{BET}) and total pore volume (V_{total}) reach up to 383.8 m² g⁻¹ and 0.653 cm³ g⁻¹ respectively. The pore size distribution is generated with nonlocal density functional theory (NLDFT) and the Horvath and Kawazoe (H–K) model. NH₂Py-PIP possesses abundant micropores mainly peaked at 0.6–2 nm and mesopores ranging from 2–10 nm (Figure S1, Supporting Information). Such a well-developed hierarchical pore structure is beneficial to facilitate enhanced mass transfer during the adsorption process. In contrast, DVB-PIP presents a typical microporous structure with a similar surface area (392.0 m² g⁻¹) but a lower V_{total} value (0.213 vs 0.653 cm³ g⁻¹), possibly leading to poor adsorption. The N₂ isotherms collected at 77 K and the CO₂ isotherms at 195 K also confirm the different character of the porosity between NH₂Py-PIP and DVB-PIP (Figure S2, Supporting Information). Scanning electron microscopy (SEM) images reveal that NH₂Py-PIP has an obvious foam-like porous structure with interconnected nanometer aggregates (Figure S3, Supporting Information). Therefore, the incorporation of the nitrogen-enriched cross-linker NH₂Py contributes to the construction of porous ionic polymers with high-degree functionality and improved porosity. As-synthesized ionic polymer NH₂Py-PIP not only possesses abundant functional sites but also exhibits a hierarchical porous structure.

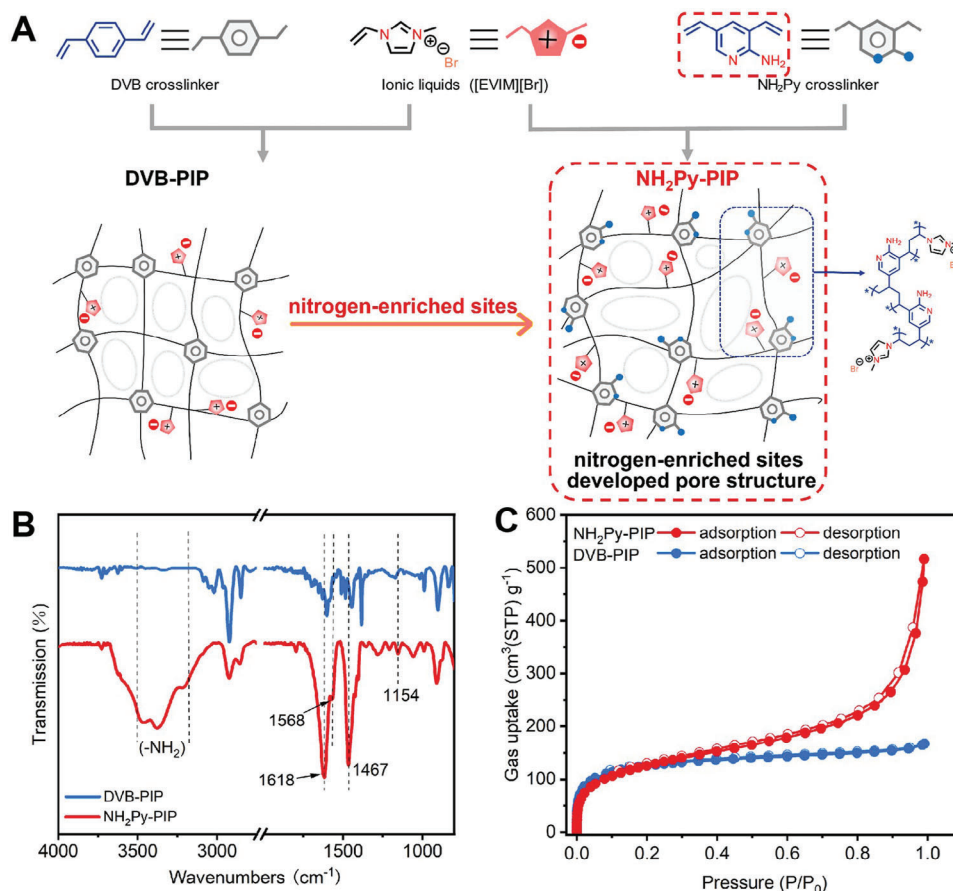


Figure 1. A) Molecular structure of the monomer of nitrogen-enriched porous ionic polymer $\text{NH}_2\text{Py-PIP}$. B) FTIR results of $\text{NH}_2\text{Py-PIP}$ and DVB-PIP. C) Ar adsorption-desorption isotherms for $\text{NH}_2\text{Py-PIP}$ and DVB-PIP at 87 K.

2.2. Gas Adsorption and Separation Performance

The unique pore chemistry and tailored pore structure of $\text{NH}_2\text{Py-PIP}$ prompt us to evaluate its desulfurization performance. The SO_2 adsorption isotherms on this ionic porous polymer were systematically collected (Figure 2A; Figure S7, Supporting Information). $\text{NH}_2\text{Py-PIP}$ presents high adsorption of SO_2 in the low-pressure region. The SO_2 uptake capacity reaches up to 1.13 mmol g^{-1} at 2000 ppm and 298 K and even increases to 1.70 mmol g^{-1} at 273 K. In contrast, as shown in Figure 2A, DVB-PIP, which has a lower nitrogen content and ionic content possesses different SO_2 capture behavior with negligible uptake ($\approx 0.06 \text{ mmol g}^{-1}$ at 2000 ppm and 298 K). For comparison, we further synthesized a nitrogen-functionalized porous polymer, PNH_2Py , with similar content of nitrogen sites (theoretical value, 17.4 wt%) and BET surface area ($331 \text{ m}^2 \text{ g}^{-1}$) via self-polymerization of pure NH_2Py . $\text{NH}_2\text{Py-PIP}$ also exhibits higher SO_2 uptake than that of PNH_2Py (1.13 vs 0.83 mmol g^{-1} at 2000 ppm) (Figure S5, Supporting Information). The superior SO_2 capture performance indicates the presence of stronger interaction in $\text{NH}_2\text{Py-PIP}$, attributed to higher-content basic nitrogen sites collaborating with abundant ionic liquid moieties. In addition, the low-concentration SO_2 uptake of $\text{NH}_2\text{Py-PIP}$ exceeds those of the reported ionic polymers,

such as the nonporous ionic liquid polymer $\text{P}(\text{D}[\text{VImC}_6]\text{Br})^{[12]}$ (0.10 mmol g^{-1}) and $\text{P}(\text{EVIMBr})^{[16]}$ (0.23 mmol g^{-1}), porous $\text{HNIP-TBMB-1}^{[17]}$ (0.63 mmol g^{-1}), and ranks only behind the best-behaving porous ionic polymers, including $\text{P}(\text{Ph-3MVIIm-Br})^{[16]}$ (1.20 mmol g^{-1}), $\text{P}(\text{Ph-4MVIIm-Br})^{[16]}$ (1.55 mmol g^{-1}), and $\text{Viologen-POF}^{[13]}$ (1.45 mmol g^{-1}) (Table S4, Supporting Information). The SO_2 uptake of $\text{NH}_2\text{Py-PIP}$ is also comparable to those of some high-performance materials such as $\text{ZU-801}^{[18]}$ (1.44 mmol g^{-1}) and $\text{SIFSIX-3-Ni}^{[19]}$ (1.39 mmol g^{-1}). Moreover, upon increasing the pressure to 0.1 bar, the SO_2 adsorption capacity of $\text{NH}_2\text{Py-PIP}$ reaches 3.85 mmol g^{-1} at 298 K. The ultimate capacity is up to 8.80 mmol g^{-1} at 1 bar and 298 K, which is approximately twice as high as that of DVB-PIP (4.26 mmol g^{-1}) with low pore volume and poor functionality. These results reveal that a precisely constructed SO_2 -affinity environment, featuring a high content of tailored nitrogen sites and abundant ionic sites, achieves underlying capture of SO_2 , and a well-developed pore structure further improves the uptake capacity.

To investigate the selective SO_2 adsorption performance of these porous ionic polymers, we measured the single-component adsorption isotherms of CO_2 , CH_4 , and N_2 at 298 K (Figure 2B; Figures S4 and S5, Supporting Information). $\text{NH}_2\text{Py-PIP}$ affords an uptake capacity of 0.91 mmol g^{-1} of CO_2 at 1 bar and 298 K, which is much lower than SO_2 adsorption capacity

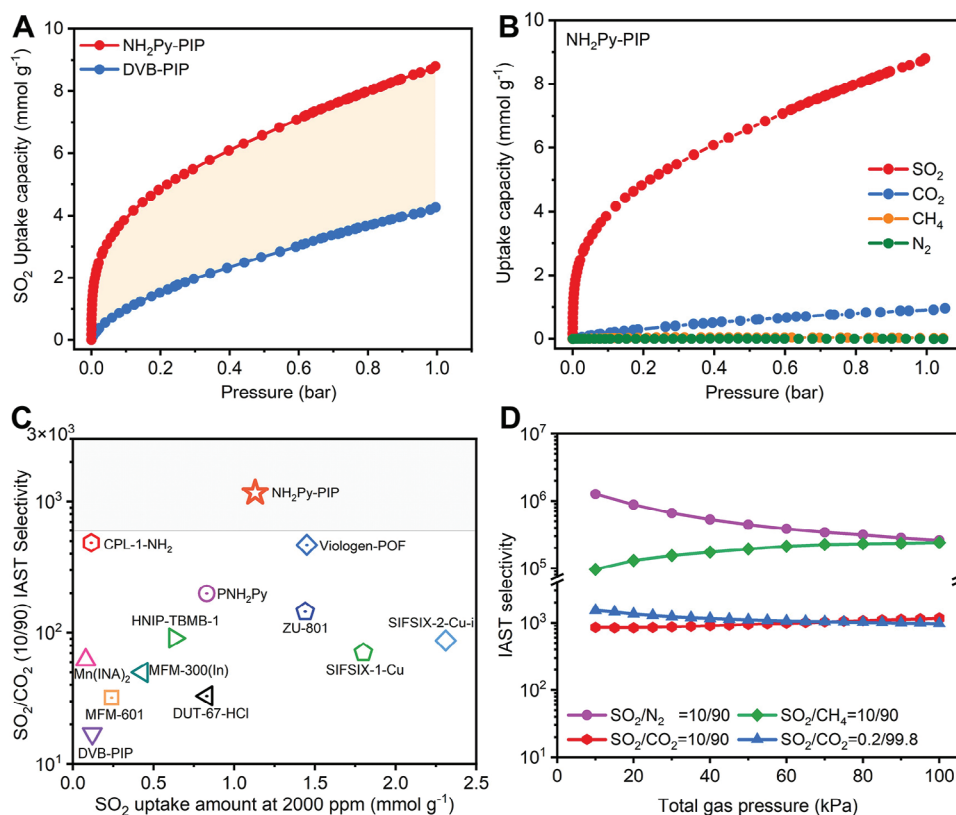


Figure 2. A) SO_2 adsorption isotherms for $\text{NH}_2\text{Py-PIP}$ and DVB-PIP at 298 K. B) SO_2 , CO_2 , CH_4 , and N_2 adsorption isotherms for $\text{NH}_2\text{Py-PIP}$ at 298 K. C) Comparison of SO_2/CO_2 (10/90) IAST selectivities and SO_2 uptake amount at 2000 ppm of good-performing SO_2 capture materials. D) SO_2/CO_2 , SO_2/CH_4 , and SO_2/N_2 IAST selectivities on $\text{NH}_2\text{Py-PIP}$ under different SO_2 partial pressure at 298 K and 1 bar.

(8.80 mmol g^{-1}). The amounts of CH_4 ($0.029 \text{ mmol g}^{-1}$) and N_2 ($0.001 \text{ mmol g}^{-1}$) absorbed are even negligible. To estimate the potential for SO_2 removal from different binary gas mixtures, the SO_2/CO_2 selectivity was determined using the ideal adsorbed solution theory (IAST). This material exhibits an extremely high selectivity of 1165 for SO_2/CO_2 separation for binary SO_2/CO_2 mixtures (10/90, v/v). As shown in Figure 2C, $\text{NH}_2\text{Py-PIP}$ presents remarkably superior SO_2/CO_2 separation performance compared with non-functional porous ionic polymer DVB-PIP (selectivity: 17), because high-density SO_2 affinity sites contribute to strong capture capacity on $\text{NH}_2\text{Py-PIP}$. Some reported adsorbents like $\text{CTF-CSU41}^{[15]}$ and $\text{POP-Pyl}^{[20]}$ prove that the introduction of nitrogen-rich or oxygen-rich functionalities could enhance the host-guest interactions. For $\text{NH}_2\text{Py-PIP-2}$, the CO_2 uptake capacity was only 0.34 mmol g^{-1} at 1 bar and 298 K (Figure S22, Supporting Information), with SO_2/CO_2 selectivity of 1651. The SO_2/CO_2 selectivity of $\text{NH}_2\text{Py-PIP}$ far exceeds those of nitrogen-functionalized porous polymers without ionic sites including PNH_2Py (199), $\text{POP-Pyl}^{[20]}$ (19.5), and $\text{P(DVB-VP)-1}^{[21]}$ (117), because these latter materials lack task-specific SO_2 recognition sites, leading to co-adsorption of CO_2 . The selectivity of $\text{NH}_2\text{Py-PIP}$ is also markedly higher than those of the previously reported porous ionic polymers such as $\text{Viologen-POF}^{[13]}$ (467) and $\text{HNIP-TBMB-1}^{[17]}$ (91), as well as benchmark MOF materials, including $\text{CPL-1-NH}_2^{[24]}$ (485), $\text{Mg-gallate}^{[22]}$ (325), $\text{ZU-801}^{[18]}$ (145), $\text{Co-gallate}^{[22]}$ (143), $\text{PCN-25 (Fe)}^{[8]}$ (37), DUT-67-

$\text{HCl}^{[26]}$ (33) and $\text{Zr-TPA-FA}^{[9]}$ (20.6) (Table S4, Supporting Information). Moreover, for $\text{NH}_2\text{Py-PIP}$, the IAST selectivities of SO_2/CH_4 and SO_2/N_2 are as high as $\approx > 10^4$ (Figure 2D). Moreover, the isosteric adsorption heat (Q_{st}) of SO_2 was calculated as 47.4 kJ mol^{-1} based on the virial equation, which is close to many top-performing adsorbents, such as SIFSIX-2-Cu-i (38.1 kJ mol^{-1}),^[19] Co-gallate (54.1 kJ mol^{-1}),^[22] functionalized porous polymers such as Viologen-POF (38.3 kJ mol^{-1}),^[13] CTF-CSU41 (44.6 kJ mol^{-1}),^[15] indicative of physical interaction between $\text{NH}_2\text{Py-PIP}$ and SO_2 (Figures S16 and S17, Supporting Information).

2.3. Dynamic Breakthrough and Recycling Experiments

Dynamic breakthrough experiments were executed to further reveal the feasibility of $\text{NH}_2\text{Py-PIP}$ for separating SO_2 from low-concentration SO_2 mixture gases, utilizing SO_2 , CO_2 , and/or N_2 mixture gases as feed. For an SO_2/CO_2 mixture containing 2000 ppm CO_2 , $\text{NH}_2\text{Py-PIP}$ presents highly effective SO_2 adsorptive removal performance (Figure 3A). SO_2 could be adsorbed until 977 min g^{-1} at a flow rate of 16.8 mL min^{-1} , with a very short breakthrough time for CO_2 . Subsequently, the SO_2 uptake capacity quickly reaches equilibrium at 1208 min g^{-1} , with a dynamic adsorption capacity up to 1.47 mmol g^{-1} , which indicates fast mass transfer, probably due to the well-developed porous

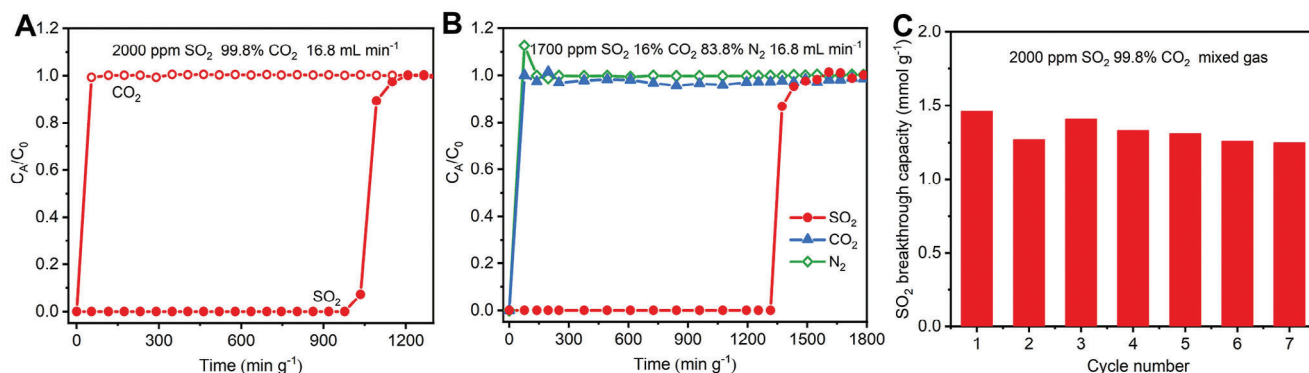


Figure 3. A) The breakthrough experiments curves of $\text{NH}_2\text{Py-PIP}$ for SO_2/CO_2 (SO_2/CO_2 , 2000 ppm/99.8%, v/v; gas flow: 16.8 mL min⁻¹) at 298 K. B) The experimental column breakthrough curves of $\text{NH}_2\text{Py-PIP}$ for $\text{SO}_2/\text{CO}_2/\text{N}_2$ (1700 ppm SO_2 , 16% CO_2 , 83.83% N_2 ; gas flow: 16.8 mL min⁻¹) at 298 K. C) The cycling breakthrough experiments of $\text{NH}_2\text{Py-PIP}$ for SO_2/CO_2 separation at 298 K.

structure. Efficient separation was also achieved with a binary SO_2/N_2 mixture containing 2000 ppm SO_2 (Figure S9, Supporting Information), N_2 breakthrough occurs at the very beginning because of its negligible adsorption, along with a long retention time for SO_2 (1091 min g⁻¹). Furthermore, for the ternary $\text{SO}_2/\text{CO}_2/\text{N}_2$ mixture (1700 ppm/16.8%/83.8% v/v/v) (Figure 3B), the breakthrough time of SO_2 is 1315 min g⁻¹, while CO_2 and N_2 elute at the very beginning. Moreover, cycling column breakthrough and SO_2 static adsorption experiments were conducted to evaluate repeatability (Figure 3C; Figure S15, Supporting Information). The SO_2/CO_2 separation performance can be well retained even after seven adsorption/desorption cycles (Figure 3C). Thermal gravimetric analysis (TGA) results demonstrate that only a 2.2 wt.% weight loss occurs at 573 K for $\text{NH}_2\text{Py-PIP}$ under an N_2 atmosphere (Figure S10, Supporting Information). The N_2 adsorption isotherms and FTIR spectra are collected before and after SO_2 adsorption, and basically, consistent results verify the structural and compositional changes in the material (Figures S11–S18, Supporting Information). The well-preserved chemical structure after the pristine material soaked in water at 373 K for one week further confirms the hydrothermal stability of $\text{NH}_2\text{Py-PIP}$ (Figure S11, Supporting Informa-

tion). These tests demonstrate that $\text{NH}_2\text{Py-PIP}$ is achievable for highly selective and reversible SO_2 adsorption with high stability, making it competitive for actual applications.

2.4. Molecular Simulation Studies

To gain a deep understanding of the interaction between the task-specific recognition sites in $\text{NH}_2\text{Py-PIP}$ and the gas molecules, density-functional theory (DFT) calculations were executed (Figure 4). A fragment consisting of the cross-linker NH_2Py and ionic unit [EVIM][Br] was utilized for calculation, which is also termed $\text{NH}_2\text{Py-PIP}$ for convenience. In the optimized geometry of the complex of $\text{NH}_2\text{Py-PIP-SO}_2$, SO_2 molecules are mainly bound by both nitrogen sites in NH_2Py and bromide anions (Br^-) in [EVIM][Br] through electrostatic interactions (Figure 4A). Despite the similar acidic properties of SO_2 and CO_2 , the BSSE (basis set superposition error)-corrected interaction energy (ΔE) between $\text{NH}_2\text{Py-PIP}$ and SO_2 is calculated as $-58.5 \text{ kJ mol}^{-1}$, this value is markedly higher than that for $\text{NH}_2\text{Py-PIP}$ and CO_2 ($-22.8 \text{ kJ mol}^{-1}$). This result indicates that the recognition sites in NH_2Py and [EVIM][Br] have stronger

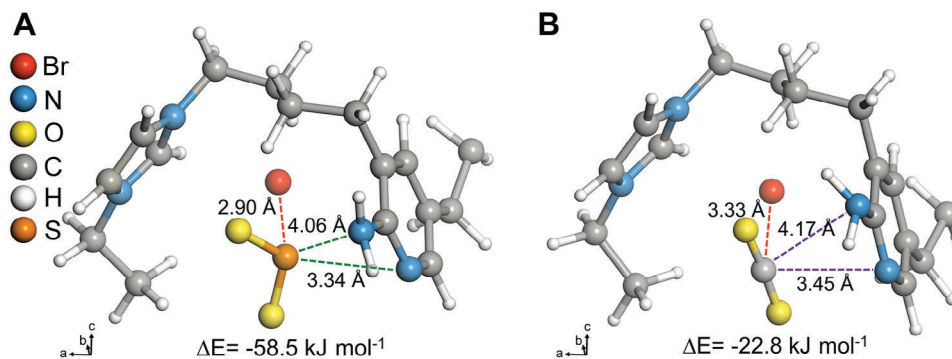


Figure 4. Quantum chemistry calculation results based on DFT theory of copolymerization unit for $\text{NH}_2\text{Py-PIP}$. Optimized structures of A) $\text{NH}_2\text{Py-PIP-SO}_2$ and B) $\text{NH}_2\text{Py-PIP-CO}_2$, ΔE (kJ mol^{-1}) is the interaction energy corrected by BSSE between $\text{NH}_2\text{Py-PIP}$ and SO_2/CO_2 . The dashed lines indicate interatomic distances (Å) between $\text{NH}_2\text{Py-PIP}$ and the gases. Color code: Br, red; N, blue; O, yellow; C, gray-40%; H, gray-10%; S, orange.

affinities for SO₂ than for CO₂. Besides, electrostatic potential energy calculation results demonstrate that for NH₂Py fragment, the N on the amino group contributes for efficiently recognizing SO₂ from CO₂, and N on the pyridine ring cooperatively improves SO₂ adsorption capacity (Table S5, Supporting Information). Additionally, FTIR spectra present the peaks at 1252 and 1114 cm⁻¹ observed after adsorption, which is assigned to the characteristic absorption peaks of S=O stretching vibration in the adsorbed SO₂ molecules (Figure S11, Supporting Information). These results reveal that SO₂ molecules are physically adsorbed on NH₂Py-PIP, and the material structure remains stable after adsorption.^[18]

3. Conclusion

In summary, we propose a feasible strategy for constructing a novel class of nitrogen-enriched porous ionic polymers, NH₂Py-PIP. Nitrogen-functionalized NH₂Py has been employed as a cross-linker for the first time in porous ionic polymers, which effectively promotes the incorporation of ionic sites and improves the porous structure. NH₂Py-PIP features high-content nitrogen sites (15.9 wt.%) and adequate ionic sites (1.22 mmol g⁻¹), coupled with a well-developed hierarchical pore structure, which addresses the trade-off issue between functionality and porosity. With fine-tuning of the SO₂-affinity environment, this material achieves both high SO₂ adsorption capacity (1.13 mmol g⁻¹ at 0.002 bar) as well as superior SO₂/CO₂ selectivity (1165), which are attributed to the task-specific recognition interactions of functional nitrogen sites and bromide anions. Real-time breakthrough experiments demonstrate that NH₂Py-PIP achieves excellent and reversible dynamic separation of SO₂ at low SO₂ concentration, and the performance could be well retained after seven cycles. This work represents a successful example of a target-motivated functionalization strategy for rationally constructing porous ionic polymers and enables to inspire the precise design of advanced adsorbents for challenging gas separations.

4. Experimental Section

Materials and Reagents: None of the chemicals had been further purified. 3,5-dibromopyridin-2-amine (98%) and azobisisobutyronitrile (AIBN, 99%, recrystallized) were purchased from Aladdin. Tetrakis(triphenylphosphine)palladium(0) (Pd(PPh₃)₄, 99%), 1-vinyl-3-ethylimidazolium bromide ([EVIM][Br], 98.5%) and potassium vinyltrifluoroborate (>97%) were obtained from Energy Chemical. Potassium carbonate (K₂CO₃, 99%) was purchased from 9dingchem. Divinylbenzene (DVB, 80%) was obtained from Sigma-Aldrich. Sodium sulfate (Na₂SO₄, 99%), ethyl acetate (99.5%), *n*-Hexane (97%), toluene (99.5%), triethylamine (99%), tetrahydrofuran (99%), and ethanol (EtOH, 99.7%) were purchased from Sinopharm.

N₂ (99.999%), SO₂ (99.99%), CO₂ (99.999%), He (99.999%), and CH₄ (99.99%) were purchased for adsorption measurements. Mixed gases of SO₂/N₂ = 2000 ppm/99.8% (v/v), and SO₂/CO₂ = 2000 ppm/99.8% (v/v) were purchased from Shanghai Wetry (China).

Synthesis of Nitrogen-Enriched Cross-linker NH₂Py: Nitrogen-enriched cross-linker 3,5-divinylpyridin-2-amine (NH₂Py) was synthesized in the following way^[25]: a mixture of potassium vinyl trifluoroborate (0.66 g, 4.8 mmol), 3,5-dibromopyridin-2-amine (0.5 g, 2.0 mmol), K₂CO₃ (0.8 g, 6.0 mmol), and Pd(PPh₃)₄ (0.058 g, 0.05 mmol) along with tetrahydrofuran (12.5 mL), toluene (12.5 mL), and H₂O (5 mL) were mixed and dis-

solved first, then refluxed under N₂ condition at 363 K for 48 h. The powder was extracted with ethyl acetate, rinsed using salt water, dried with Na₂SO₄, and treated by vacuum evaporation. The eluent was composed of ethyl acetate, *n*-hexane, and triethylamine (50/50/3, v/v/v), then purified by flash chromatography to obtain a light red powder. ¹H NMR (400 MHz, CDCl₃-d, ppm), δ = 8.01 (d, Py-H, 1H), 7.60 (d, Py-H, 1H), 6.62 (ddd, -CH=, 2H), 5.69 (dd, =CH₂, 1H), 5.61 (d, =CH₂, 1H), 5.42 (dd, =CH₂, 1H), 5.15 (d, =CH₂, 1H), 4.62–4.58 (m, -NH₂, 2H). ¹³C NMR (101 MHz, DMSO-d₆, ppm) δ = 156.61, 146.65, 133.68, 131.55, 129.60, 122.33, 116.11, 115.47, 110.50; Elemental analysis (CHN) for NH₂Py (C₉N₂H₁₀): N (wt.%) 17.39, C (wt.%) 72.70, H (wt.%) 6.71.

Synthesis of Nitrogen-Functionalized Porous Ionic Polymers and Comparison Materials: NH₂Py-PIP was synthesized as follows: NH₂Py (1.00 g, 6.8 mmol), [EVIM][Br] (0.0875 g, 0.425 mmol), and AIBN (0.034 g) were dissolved in 10 mL ethyl acetate/ethyl alcohol/water (v/v/v = 8/4/2) in a 50 mL Schlenk bottle and were thoroughly mixed by stirring at ambient temperature for 2 h. After treatment at 353 K for one day under nitrogen protection, the product was washed using ethyl acetate, followed by drying under vacuum at 353 K for one day. NH₂Py-PIP-2 was synthesized using the molar ratio of NH₂Py to [EVIM][Br] to 2:1. The non-ionic-functionalized PNH₂Py was self-polymerized by NH₂Py in the same way.

Single-Component Gas Sorption Experiments: The activated adsorbent samples were obtained after being vacuumed at 373 K for 12 h. SO₂ and Ar sorption isotherms were gathered at 273, 298, 313, and 87 K using BSD-PMC Corrosive Gas Adsorption Analyzer (BSD Instrument Crop). CO₂, N₂, and CH₄ isotherms were gathered at 298 K using ASAP 2460 (Micromeritics Corp).

Dynamic Column Breakthrough Tests: The breakthrough tests were accomplished with lab-scale fixed-bed equipment. Column (inner diameter × length = 4.6 mm × 30 mm) used as test vessel. The mass of NH₂Py-PIP was 0.0872 g. The binary SO₂/CO₂ (2000 ppm/99.8%, v/v) mixture with gas flow of 16.8 mL min⁻¹ was used as feed, SO₂/N₂ (2000 ppm/99.8%, v/v) corresponded to 20 mL min⁻¹, simulated flue gas SO₂/CO₂/N₂ (2000 ppm/16%/83.8% v/v/v) corresponded to 16.8 mL min⁻¹. Outlet components from the packed bed were detected by thermal conductivity detector (TCD) and gas chromatography (GC-2010 plus). For regeneration, this column was heated at 373 K with helium (He) at the flow rate of 20 mL min⁻¹ for 12 h.

Supporting Information

Supporting Information is available from the Wiley Online Library or from the author.

Acknowledgements

S.C. and S.H. contributed equally to this work. This work was supported by the National Natural Science Foundation of China (No. 22122811, 22278354, and 21938011), and the Shanxi-Zheda Institute of Advanced Materials and Chemical Engineering (Grant No. 2021SZ-TD008). The authors also acknowledge the Research Computing Center in the College of Chemical and Biological Engineering at Zhejiang University.

Conflict of Interest

The authors declare no conflict of interest.

Data Availability Statement

The data that support the findings of this study are available in the supplementary material of this article.

Keywords

adsorption, functionalization, gas separation, porous ionic polymers, sulfur dioxide

Received: January 30, 2024
Revised: April 1, 2024
Published online:

- [1] a) J. K. Sun, M. Antonietti, J. Y. Yuan, *Chem. Soc. Rev.* **2016**, *45*, 6627; b) D. Xu, J. N. Guo, F. Yan, *Prog. Polym. Sci.* **2018**, *79*, 121; c) J. F. Xiong, X. W. Wang, L. L. Li, Q. N. Li, S. J. Zheng, Z. Y. Liu, W. Z. Li, F. Yan, *Angew. Chem., Int. Ed.* **2024**, *63*, e202316375; d) L. Q. Qiu, H. G. Peng, Z. Z. Yang, J. T. Fan, M. J. Li, S. Z. Yang, D. M. Driscoll, L. R., S. M. Mahurin, L. N. He, S. Dai, *Adv. Mater.* **2023**, *35*, 2302525.
- [2] a) T. Zhou, X. Y. Huang, N. Ding, Z. Liu, Y. Yao, J. Guo, *Chem. Soc. Rev.* **2022**, *51*, 237; b) X. H. Li, Y. L. Wang, J. Wen, L. L. Zheng, C. Qian, Z. H. Cheng, H. Y. Zuo, M. Q. Yu, J. Y. Yuan, R. Li, W. Y. Zhang, Y. Z. Liao, *Nat. Commun.* **2023**, *14*, 263; c) P. H. Zhang, Z. F. Wang, P. Cheng, Y. Chen, Z. J. Zhang, *Coord. Chem. Rev.* **2021**, *438*, 213873; d) H. Y. Jiang, T. T. Li, L. Bai, J. L. Han, X. C. Zhang, H. F. Dong, S. J. Zeng, S. J. Luo, X. P. Zhang, *ACS Appl. Mater. Interfaces* **2023**, *15*, 51204; e) X. Suo, Y. Q. Fu, C. L. D. Thanh, L. Q. Qiu, D. E. Jiang, S. M. M., Z. Z. Yang, S. Dai, *J. Am. Chem. Soc.* **2022**, *144*, 21658.
- [3] a) K. Wang, W. W. Cui, Z. Y. Bian, Y. Q. Liu, S. Jiang, Y. Zhou, J. Wang, *Appl. Catal. B* **2021**, *281*, 119425; b) D. Luo, M. Li, Q. Y. Ma, G. B. Wen, H. Z. Dou, B. H. Ren, Y. Z. Lin, X. Wang, L. L. Shui, Z. W. Chen, *Chem. Soc. Rev.* **2022**, *51*, 2917; c) S. J. Zeng, X. P. Zhang, L. Bai, X. C. Zhang, H. Wang, J. J. Wang, D. Bao, M. D. Li, X. Y. Liu, S. J. Zhang, *Chem. Rev.* **2017**, *117*, 9625; d) S. Fischer, A. schimanowitz, R. Dawson, I. Senkowska, S. Kaskel, A. Thomas, *J. Mater. Chem. A* **2014**, *2*, 11825.
- [4] a) G. Q. Li, S. Dong, P. Fu, Q. H. Yue, Y. Zhou, J. Wang, *Green Chem.* **2022**, *24*, 3433; b) X. J. Li, J. Q. Wang, Q. Yuan, X. G. Song, J. L. Mu, Y. Wei, L. Yan, F. F. Sun, Y. T. Cai, Z. Jiang, Z. K. Han, Y. J. Ding, *Angew. Chem., Int. Ed.* **2023**, *62*, e202307570; c) M. Yi, M. Wang, Y. Wang, Y. L. Wang, J. Chang, A. K. Kheirabad, H. Y. He, J. Y. Yuan, M. Zhang, *Angew. Chem., Int. Ed.* **2022**, *61*, e202202515; d) X. Suo, Y. Q. Huang, Z. K. Li, H. Q. Pan, X. L. Cui, H. B. Xing, *Sci. China Mater.* **2022**, *65*, 1068.
- [5] a) O. Guselnikova, O. Semyonov, E. Sviridova, R. Gulyaev, A. Gorbunova, D. Kogolev, A. Trelin, Y. Yamauchi, R. Boukherroub, P. Postnikov, *Chem. Soc. Rev.* **2023**, *52*, 4755; b) L. Q. Qiu, L. Peng, D. Moitra, H. J. Liu, Y. Q. Fu, Z. Dong, W. D. Hu, M. Lei, D. E. Jiang, H. F. Lin, J. Z. Hu, K. A. McGarry, I. Popovs, M. Li, A. S. Ivanov, Z. Z. Yang, S. Dai, *Small* **2023**, *19*, 2370338.
- [6] a) X. Suo, X. L. Cui, L. F. Yang, N. Xu, Y. Q. Huang, Y. He, S. Dai, H. B. Xing, *Adv. Mater.* **2020**, *32*, 1907601; b) L. Luo, J. R. Li, X. Y. Chen, X. G. Cao, Y. B. Liu, Z. X. Wu, X. Y. Luo, C. M. Wang, *Chem. Eng. J.* **2022**, *427*, 131638; c) J. Y. Cui, Z. Q. Zhang, L. F. Yang, J. B. Hu, A. Y. Jin, Z. L. Yang, Y. Zhao, B. Meng, Y. Zhou, J. Wang, Y. Sun, J. Wang, X. L. Cui, H. B. Xing, *Science* **2023**, *383*, 179; d) H. Q. Pan, X. Suo, Z. L. Yang, L. Y. Chen, X. L. Cui, H. B. Xing, *Sep. Purif. Technol.* **2021**, *279*, 119728.
- [7] a) J. W. Li, C. Wang, H. Y. Wu, J. X. Zhang, M. Zhang, Q. Zhu, Y. Q. Fan, H. Liu, W. S. Zhu, *Energy Fuels* **2023**, *37*, 8051; b) X. Kan, G. Q. Zhang, J. Ma, F. Q. Liu, Y. Tang, F. J. Liu, X. F. Yi, Y. F. Liu, A. M. Zheng, L. L. Jiang, F. S. Xiao, S. Dai, *Adv. Funct. Mater.* **2024**, 2312044, <https://doi.org/10.1002/adfm.202312044>; c) L. F. Luo, W. J. Zhang, C. Song, J. T. Tang, F. Y. Hu, J. Pan, Y. B. Zhang, C. Y. Pan, G. P. Yu, X. G. Jian, *Ind. Eng. Chem. Res.* **2022**, *61*, 9785.
- [8] a) S. H. Chen, Y. Wu, W. X. Zhang, S. S. Wang, T. Yan, S. J. He, B. L. Yang, H. P. Ma, *Chem. Eng. J.* **2022**, *429*, 132480; b) G. L. Smith, J. E. Eyley, X. Han, X. R. Zhang, J. N. Li, N. M. Jacques, H. G. W. Godfrey, S. P. Argent, L. J. M. Mcpherson, S. J. Teat, Y. Q. Cheng, M. D. Frogley, G. Cinque, S. J. Day, C. C. Tang, T. L. Easun, S. Rudić, A. J. Ramirez-Cuesta, S. H. Yang, M. Schröder, *Nat. Mater.* **2019**, *18*, 1358; c) H. C. Lan, J. Y. Zhang, Q. J. Dai, H. Ye, X. Y. Mao, Y. C. Wang, H. L. Peng, J. Du, K. Huang, *Chem. Eng. J.* **2021**, *409*, 127378; d) J. Z. Yao, Z. W. Zhao, L. Yu, J. J. Huang, S. G. Shen, S. Y. Zhao, Y. Wu, X. Y. Tian, J. Wang, Q. B. Xia, *J. Mater. Chem. A* **2023**, *11*, 14728.
- [9] a) Z. H. Zhang, B. L. Yang, H. P. Ma, *Sep. Purif. Technol.* **2021**, *259*, 118164; b) W. L. Xu, L. J. Li, M. W. Guo, F. Z. Zhang, P. C. Dai, X. Gu, D. D. Liu, T. Liu, K. T. Zhang, T. Xing, M. Z. Wang, Z. Li, M. B. Wu, *Angew. Chem., Int. Ed.* **2023**, *13*, e202312029; c) S. Q. Gang, Z. Y. Liu, Y. N. Bian, R. H. Wang, J. L. Du, *Sep. Purif. Technol.* **2024**, *335*, 126153; d) W. Gong, Y. Xie, A. Yamano, S. Ito, X. H. Tang, E. W. Reinheimer, C. D. Malliakas, J. Q. Dong, Y. Cui, O. K. Farha, *J. Am. Chem. Soc.* **2023**, *145*, 26890.
- [10] a) S. T. Parker, A. Smith, A. C. Forse, W. C. Liao, F. B. Altvater, R. L. Siegelman, E. J. Kim, N. A. Zill, W. J. Zhang, J. B. Neaton, J. A. Reimer, J. R. Long, *J. Am. Chem. Soc.* **2022**, *144*, 19849; b) R. M. Main, S. M. Vornholt, R. Ettliger, P. Netzsch, M. G. Stanzione, G. M. Rice, C. Elliott, S. E. Russell, M. R. Warren, S. E. Ashbrook, R. E. Morris, *J. Am. Chem. Soc.* **2024**, *146*, 3270.
- [11] H. Tao, G. L. Shi, L. L. Jiang, W. J. Lin, H. R. Li, C. M. Wang, *Sep. Purif. Technol.* **2024**, *333*, 125974.
- [12] L. Xia, Q. Cui, X. Suo, Y. H. Li, X. L. Cui, Q. W. Yang, J. H. Xu, Y. W. Yang, H. B. Xing, *Adv. Funct. Mater.* **2018**, *28*, 1704292.
- [13] S. S. Wang, Y. Wu, X. Y. Li, W. X. Zhang, H. P. Ma, *ACS Appl. Mater. Interfaces* **2023**, *15*, 30312.
- [14] a) C. Wang, H. Y. Wu, J. W. Li, J. R. Zhang, J. X. Zhang, J. C. Ding, H. P. Li, W. S. Zhu, *Chem. Eng. J.* **2023**, *471*, 144394; b) D. Li, Y. Kang, *J. Hazard. Mater.* **2021**, *404*, 124101.
- [15] Y. Fu, Z. Q. Wang, S. Z. Li, X. M. He, C. Y. Pan, J. Yan, G. P. Yu, *ACS Appl. Mater. Interfaces* **2018**, *10*, 36002.
- [16] X. Suo, Y. Yu, S. H. Qian, L. Zhou, X. L. Cui, H. B. Xing, *Angew. Chem., Int. Ed.* **2021**, *60*, 6986.
- [17] X. C. An, Z. M. Li, Y. Zhou, W. S. Zhu, D. J. Tao, *Chem. Eng. J.* **2020**, *394*, 124859.
- [18] C. Yu, P. X. Zhang, Q. Ding, L. F. Yang, X. Suo, X. L. Cui, H. B. Xing, *Chem. Eng. J.* **2023**, *471*, 144768.
- [19] X. L. Cui, Q. W. Yang, L. F. Yang, R. Krishna, Z. G. Zhang, Z. B. Bao, H. Wu, Q. L. Ren, W. Zhou, B. L. Chen, H. B. Xing, *Adv. Mater.* **2017**, *29*, 1606929.
- [20] Z. F. Dai, W. Chen, X. Kan, F. Y. Li, Y. F. Bao, F. Zhang, Y. B. Xiong, X. J. Meng, A. M. Zheng, F. S. Xiao, F. J. Liu, *ACS Macro Lett.* **2022**, *11*, 999.
- [21] Y. Zhou, M. Z. Cai, X. J. Shu, Z. H. Xu, L. S. Zhou, X. K. Wu, *Chem. Eng. J.* **2022**, *435*, 134876.
- [22] F. Q. Chen, D. Lai, L. D. Guo, J. Wang, P. X. Zhang, K. Y. Wu, Z. G. Zhang, Q. W. Yang, Y. W. Yang, B. L. Chen, Q. L. Ren, Z. B. Bao, *J. Am. Chem. Soc.* **2021**, *143*, 9040.
- [23] L. Li, I. Da Silva, D. I. Kolokolov, X. Han, J. G. Li, G. Smith, Y. Q. Cheng, L. L. Daemen, C. G. Morris, H. G. W. Godfrey, N. M. Jacques, X. R. Zhang, P. Manuel, M. D. Frogley, C. A. Murray, A. J. Ramirez-Cuesta, G. Cinque, C. C. Tang, A. G. Stepanov, S. H. Yang, M. Schroder, *Chem. Sci.* **2019**, *10*, 1472.
- [24] Z. D. Guo, Y. J. Li, P. X. Zhang, J. Y. Cui, L. Y. Chen, L. F. Yang, J. Wang, X. L. Cui, H. B. Xing, *Sep. Purif. Technol.* **2022**, *295*, 121337.
- [25] M. Savage, Y. Q. Cheng, T. L. Easun, J. E. Eyley, S. P. Argent, M. R. Warren, W. Lewis, C. Murray, C. C. Tang, M. D. Frogley, G. Cinque, J. L. Sun, S. Rudic, R. T. Murden, M. J. Benham, A. N. Fitch, A. J. Blake, A. J. Ramirez-Cuesta, S. H. Yang, M. Schroder, *Adv. Mater.* **2016**, *28*, 8705.
- [26] X. H. Xiong, Z. W. Wei, W. Wang, L. L. Meng, C. Y. Su, *J. Am. Chem. Soc.* **2023**, *145*, 14354.
- [27] Y. P. Song, Q. Sun, B. Aguila, S. Q. Ma, *Catal. Today* **2020**, *356*, 557.